Science & Technology Facilities Council

Technical Report
RAL-TR-2012-005

Electromagnetic pulse generation in petawatt laser shots

JE Bateman, MJ Mead

March 2012

RAL Library
STFC Rutherford Appleton Laboratory
R61
Harwell Oxford
Didcot
OX11 0QX

Tel: +44(0)1235 445384
Fax: +44(0)1235 446403
email: libraryral@stfc.ac.uk

Science and Technology Facilities Council reports are available online at: http://epubs.stfc.ac.uk

ISSN 1358- 6254

ELECTROMAGNETIC PULSE GENERATION IN PETAWATT LASER SHOTS

J.E.Bateman,

Science and Technology Facilities Council, Rutherford Appleton Laboratory, Harwell Science and Innovation Campus, Didcot, Oxfordshire, OX11 0QX, U.K.

M. J. Mead

Institute of Physics of the Academy of Science, Na Slovance 1999/2, 182 21 Prague 8, Czech Republic

23 March 2012

Abstract

As laser power has increased towards the petawatt region electromagnetic pulse (EMP) fields of up to 100kV/m have been recorded in the target chamber causing a real threat to the integrity of diagnostic instruments. The radiation, being in the 100MHz to >1GHz frequency band also causes more widespread interference in the laser facility. Recent work at Lawrence Livermore National Laboratory [1] points the finger at the flux of high energy (MeV) electrons leaving the target as the primary cause of the EMP. In this report we analyse a general physical model of the modality of the process which couples the two phenomena with the aim of devising mitigating strategies.

1. Introduction

The scientific case for the Extreme Light Facility (ELF) is predicated on the ability of petawatt laser pulses delivered in picosecond pulses to generate high energy x-rays (>1MeV), energetic ion beams (e.g. protons >100MeV) and ultra-short (attosecond) light pulses as well as electron beams of multi-MeV energies. All of these processes are dependent on the primary production of very hot (>MeV) electrons in the primary plasma which escape from the target region in copious ($>10^{12}$) quantities. The findings in the work described in ref. [1] that the EMP is attributable to escaping electrons rather than the neutral radiations emitted by the plasma (e.g. UV, x-rays and secondary electron created by them in the chamber walls) imply that the EMP will be an inescapable fact in virtually all ELF applications and that strategies for mitigation and accommodation must be considered as part of the design process.

In ref. [1] a sophisticated modelling process for the interaction of the escaping electrons with the target chamber is described and good agreement is obtained with the measured radiofrequency (RF) spectrum measured by the probes in the TITAN target chamber. However, a physical understanding of the mechanisms is not readily available from this approach and it is possible to use some of their data to validate a simpler physical model which can perhaps be more persuasive for adapting user attitudes and more helpful for conceiving possible mitigation measures. The need for such measures has been widely noted [2,3].

2. The Model

The model for EMP generation considered here derives from the concept of the laser target chamber as resonant cavity stimulated by a bunched fast electron beam – in other words a klystron (however inefficient). One of us (M.J.M.) has already measured and analysed the EMP in the VULCAN target chamber at Rutherford Appleton Laboratory on a similar basis [4]. In such a situation two distinct considerations arise – the properties of the target chamber as a resonator and the structure of the driving pulse of electrons. After the termination of the laser pulse (only a few ps in the applications under consideration) the motion of the electrons is ballistic and therefore the first requirement is to know the electron energy spectrum. We are fortunate to have the electron spectrometer data from the shots in the TITAN laser chamber in the report from LLNL (figure 11 in ref. [1]). In consequence we chose to analyse the TITAN target chamber idealised to a perfect cylinder and examine its possible response to the electron bunches.

2.1 The TITAN target chamber as resonator (idealised)

The TITAN target chamber is idealised as an aluminium cylinder 1m high by 1m radius. Figure 1 shows the lowest possible oscillation frequencies for such a cavity and the first 5 harmonics in each dimension, amounting to 180 E modes and 150 H modes which stretch from ~100MHz to ~1.4GHz (in an alternative nomenclature the E waves are known as TM - transverse magnetic – and the H waves as TE – transverse electric). On the ordinate is plotted the Q of the cavity for each mode. This plot indicates two important aspects of the situation – first the plethora of modes available in this frequency range and the extreme responsiveness of the cavity with Q

values $>10^5$. The plot is calculated using the relations given in ref. 5 with the Bessel function (and derivative) zeros as listed in ref. [6].

The target chamber is anything but a perfect cavity with multiple access ports through which the RF field can leak and much clutter of target station and diagnostics inside the cavity with resultant breaking up of mode structures and lossy materials. In practice amplitude decay times of typically a few hundred ns are observed [1] (in agreement with other measurements [4]). Using the relation $Q = \pi f \tau$ we see that for a typical frequency (f) of 1GHz and an amplitude decay time (τ) of 200ns Q ~ 600. However, the idealised Q value gives a useful measure of the responsiveness of the chamber to stimulation at a given frequency. The general trend of Q shows the dominant $f_m^{1/2}$ dependence of Q where f_m is the frequency of the mode. Q is also controlled by the conductivity of the cavity wall (σ) according to $\sigma^{1/2}$.

2.2 Electron Bunch Structure

Which, and how strongly the modes exhibited in Figure 1 are stimulated is governed by the time structure of the electron beam and its direction. Electrons moving normally to the chamber wall tend to stimulate E modes and those travelling parallel H modes. If electron acceleration does not have a mechanism to persist beyond the presence of the driving laser pulse (2ps in the case of the TITAN experiments), the motion of the electrons can be taken as purely ballistic and the electron energy spectra measured in ref. [1] can be used to derive the electron distribution in time. The spatial aspect is more complicated but the distributions observed [1] show that the lower energies are very approximately isotropic (i.e. form an expanding spherical shell) and the most energetic favour the beam direction. We shall ignore spatial subtleties and treat the problem as approximately spherically symmetric, concentrating on the time structure which is the dominant factor in determining the response of the chamber.

2.2.1 Electron Energy Spectra

In the study described in ref. [1] a series of high energy laser shots were fired at a 12 micron thick silver target of a range of sizes with a constant pulse length (2ps) and a constant spot diameter (~20 microns) (pulse energy not stated). The energy spectra were obtained from a series of carefully calibrated Thermo-Luminescent Detectors (TLD) fielded around the target. Care was also taken to be able to identify any gamma ray contribution and calibrate it out. The electron spectra from four shots on different target sizes are published in ref. [1] though the angle of this detector to the incident beam is not given. Limited as it is, this data provides the basic information necessary to calculate a notional bunch shape of the ballistic electron cloud in the radial direction. All the electrons originate at a small spot at a highly defined instant in time and with the caveat entered above about the spatial distribution, are treated as an expanding spherical shell.

The four spectra published in ref. [1] were digitised manually in coarse steps and fitted with a double exponential formula. Figure 2 shows all four fits to the four shots with various target sizes (0.4mm, 1mm, 3mm and 10mm) with the “data” shown only for the 10mm target. All the fits look satisfactory; while in some shots some structure can be seen in the low energy region (<1000keV) the simple exponential fits seem to

capture the behaviour of the spectra well enough for our purposes. The fitting formula used is:

$$\frac{dN}{dT_e} = \alpha e^{-T_e/T_L} + \beta e^{-T_e/T_H} \qquad (1)$$

This fit can be interpreted as fitting two distinct populations of quasi-thermalised electrons with temperatures of T_L and T_H. T_L remains relatively constant lying between 387keV (0.4mm target) and 535keV (10mm target) while T_H is much more variable ranging from 8271keV (3mm target) to 34155keV (1mm target). An inspection of Figure 2 shows that the fit to the 3mm target data does not accord well with the fits to the other shots. It is not known whether this is an artefact of the fitting caused by the (unexplained) truncation of the data presented to a maximum energy of 16000keV or a genuine physical effect. This data set stands out as anomalous-looking in all the manipulations described below.

2.2.2 Electron Kinematics

It is clear from Figure 2 that the bulk of our electrons possess kinetic energies above 511keV (m_0c^2 the rest mass of the electron expressed in energy terms which we will abbreviate to m_e). This means that the motion of the bulk of the electrons is relativistic and must be treated accordingly. Since we are interested in the time structure it is more useful to us the parameter s (=1/v) the slowness of the particle in units of ns/m in place of the velocity – v. Similarly the constant a = 1/c is used where c is the velocity of light. (The parameter a is truncated to 3.336ns/m for convenience.) The usual relativistic relations give us s as a function of T_e and T_e as a function of s:

$$s = \frac{a}{\sqrt{1-\left(\frac{1}{1+T_e/m_e}\right)^2}} \text{ ns/m} \qquad (2)$$

And conversely:

$$T_e = m_e\left\{\frac{1}{\left(1-\frac{a^2}{s^2}\right)^{1/2}}-1\right\} \text{ keV} \qquad (3)$$

Figures 3 and 4 show plots of these two relations. The electron slowness is simply interpreted as the flight time for a path of 1m which is the order of the electron flight paths to the TITAN chamber walls.

2.2.3 Electron bunch structure in time and space

We now have the tools to construct a notional bunch structure. If we evaluate dN/ds then the time structure of the bunch at any point in space is just given by multiplying this by the length of the flight path-length to that point. We apply:

$$\frac{dN}{ds} = \frac{dN}{dT_e}\frac{dT_e}{ds} \qquad (4)$$

Where dN/dT_e is one of the fits of Figure 2 and dT_e/ds is obtained by differentiating expression (3) above and substituting for s from expression (2). Figure 5 shows the outcome of this transformation which may be thought of as the time distribution of the electron bunch arriving at the chamber wall. Since $dT_e/ds \rightarrow \infty$ as $s \rightarrow a$ from above (see Figure 4) while $dN/dT_e \rightarrow 0$ dN/ds has a singularity at s = a. Thus the front edge of the plots in Figure 5 is an arbitrary vertical line at s = a. In the physical case the front edge will be defined by the time dependence of the acceleration process which (it is assumed) will little exceed the laser pulse length (2ps in the TITAN experiments).

Given the great range of dN/ds, a logarithmic scale is used for the ordinate of the plot. The distributions clearly exhibit two peaks: an initial spike (clearly due to the relativistic compression experienced by the high energy/temperature electrons) and a more spread-out distribution caused by the low temperature electrons. It is helpful to review the two distributions separately on a linear scale: Figure 6 shows the relativistic spikes on a scale in which the least significant digit on the abscissa represents 1ps. Figure 7 shows the data of Figure 5 re-plotted to show the low temperature electron distribution on a suitable scale. Markers derived from Figure 4 indicate the typical range of electron energies contributing to the two distributions.

These figures show that the two electron populations stimulate the chamber in radically different time domains – a few picoseconds (potentially - and convolved with the acceleration time scale) and a few nanoseconds. This can also be illustrated by the Fourier Transform of one of the plots in Figure 5. In Figure 8 we observe two frequency domains clearly. It is noted that the lower frequency domain overlaps closely with the lower modes of the TITAN chamber as shown in Figure 1.

Integrating the curves of Figure 5 allows us to estimate the fraction of electrons in the fast spike as a function of the target size. Figure 9 shows the result – a steady increase as the target size increases which correlates with the increase in the EMP observed in ref. [1] as the target size increased.

The above discussion has focussed on the dN/ds spectrum which simply represents the time distribution of the electron bunch after 1m of flight from the target. The time distributions of the bunch at intervening times on its way out are simply evaluated by applying the transformations $dN/dt = dN/ds / r$, $t = sr$ where r is the corresponding path length. Figure 10 shows this operation applied to the 3mm target spectrum. It is obvious that the electron bunch spreading in flight reduces its bandwidth as it retreats from the target.

Some more complicated transformations are required to derive the spatial distributions at a given flight distance from the target (we must work in terms of the velocity instead of the slowness but the derivation is similar). Figure 11 shows the result for the 3mm target spectrum, presenting “snapshots” of the notional bunch at various distances from the target.

2.3 Induction Pulse Formation

Resonant behaviour in the chamber structure begins when currents begin to flow in the structure. The fundamental process initiating such current is the ionisation of the target plasma and the subsequent charge separation that takes place as the high energy electrons leave the initial plasma. In the time scale relevant to the stimulation of the cavity (~1ns) the plasma of silver ions (in the TITAN experiments of ref. [1]) are inertially confined (their mass is ~$2x10^5$ times that of the electrons) and they hold on to the low energy electrons. Thus the expanding shell of high energy electrons leaves a fixed positive charge on the target which will eventually be neutralised by electrons flowing back up the target support from the chamber body. Of course the currents will be induced in all metal surfaces within the chamber and returned to the target by some path but for simplicity we consider just the chamber – all charge will return by it eventually. This situation is basically analogous to that in the traditional gas avalanche radiation detector where a plasma forms near the central electrode (typically a fine wire) and the drifting of the positive ions towards the outer electrode produces a characteristic time profile of the induced charge / current which is mirror imaged in each electrode. The similarity of the physical format allows us to estimate the effect of the dramatic difference in some of the parameters and get a feel for the order of magnitude of the rise time of the charge pulse induced in the chamber structure and so the type of stimulation our resonator will experience.

In the avalanche counter the moving charges are positive ions (usually argon ions) drifting at a variable (decreasing) velocity under the effect of a bias field from the anode (typically 25 microns diameter) out to a cathode cylinder at a radius of typically 10mm. In the laser shot the moving charges are negative electrons moving ballistically at close to luminal velocity. Once a few mm away from the plasma and having lost some energy by climbing out of the potential well of the positive ions their velocity will become essentially constant. In the case of the avalanche counter a simple calculation of the shape of the induced charge pulse is possible – it is based on consideration of the energy flow in the capacitor represented by the detector. Ref. 7 provides details of typical time profiles observed in different geometries. In particular we see that in a cylindrical detector of the geometry specified above ~50% of the total charge pulse is developed in ~100ns when the total drift time to clearance is ~1ms. This period of 100ns corresponds to the drift of the ions over a distance of only a few wire diameters i.e. 50 – 75 microns, a very small fraction of the total drift distance.

While the moving charge velocities are very different (the mean ion velocity in the initial drift in the counter is only ~1000m/s) the basic configuration is the same as the electrons in the laser pulse case escape from the neutralising positive ion field falling off as $1/r^2$. In other words we can expect the same configuration of charge induction pulse – a very sharp rise compared with the overall transit time (~3ns) and corresponding to movement over a very small proportion of the full transit. Thus if we take electrons of luminal velocity and estimate that a travel of ~10mm will generate a large fraction of the induction pulse we get a rise time of ~30ps. We note from Figure 7 that the peaks of even the low slow distribution of electrons are at T_e~1MeV at which energy the electron velocity is >90% luminal.

In the avalanche counter case the ion movement is so slow that the electric field can always rearrange itself as fast as the ions move. In the case of the laser pulse this is

not so. The electrons retreating from the target are moving almost as fast as their electric field can propagate. In relativistic terms this is familiar as the flattening of the particle field into a pancake shape in the transverse plane as the velocity approaches luminal leading to such familiar phenomena as transition radiation and the relativistic rise in the specific ionisation. This effect for MeV electrons can be evaluated using a worked example given in ref. 11. A snapshot of the spatial distribution of the E field of the fast electron in the laboratory frame of reference turns out to be represented by the rest field, e/r^2 multiplied by a relativistic form factor $F(\gamma,\theta)$ where $\gamma = 1 + T_e/m_e$ and θ is the (spherical) polar angle of the vector **r** to the direction of motion. The function F is shown in figure 12 where it is observed that as the electron energy rises above 0.5MeV the static field configuration is heavily modified by compression into the transverse plane. As is obvious from the formula given for F in figure 12, in the transverse plane ($\theta = 90^o$) the value of E becomes amplified to $\gamma\, e/r^2$ while in the longitudinal direction ($\theta = 0^o$) it becomes reduced to $e/r^2 / \gamma^2$. Thus in addition to the relativistic compression on the (notional) charge bunch of escaping electrons demonstrated above, we see that we have a similar compressive effect in the induction pulse which precedes the bunch leading to a strongly enhanced impulsive drive to the chamber structure.

If we take the transit to the chamber wall, then it is clear that no effect from the target can reach it in less than 3.336ns but that when information begins to arrive it arrives almost simultaneously – induction pulse only slightly ahead of the particles – if we take a minimum electron velocity of β (v/c) = 0.9 then the maximum gap between the arrival of the fast induction pulse and the fast electrons is ~333ps, though as figure 12 shows, the strongest part of the E field is pinned to the particle. The presence of metallic experimental clutter in the chamber will confuse the picture a little in providing possibly shorter flight paths and shorter return paths to the target and the lowest energy electrons (<100keV) will produce some low level stimulation at later times. However, the basic picture remains that with the emission of a pulse of relativistic electrons the chamber structure will be subjected to violent stimulation in the >1GeV frequency band with spikes capable of stimulating frequencies at least 10 times this value. (One notes that the EMP energy vs frequency spectra presented in ref. [1] show no sign of declining at their maximum measurement frequency of 5GHz.)

3. Discussion

Representing the target structure by a sphere of 1cm radius gives a capacitance of ~1pF if the chamber is of meter dimensions. In the static case, after the full collection of a charge of $5\text{x}10^{12}$ electrons (0.8μC) the potential between the target and the chamber wall is ~800kV with the field falling off as $1/r^2$ from the target. The impulsive nature of the stimulus provided by the relativistic electron bunch inevitably makes the chamber structure resonate at any of the modes open to it (the Fourier Transform of a delta function contains all frequencies). The complexities of conductor-bounded space caused by the internal instrumentation introduce a further range of possible oscillatory modes (many of which will be damped). Measuring the EMP directly within the chamber under these conditions is very challenging. The establishment of the principle that the high energy electrons are primarily responsible for the EMP, as done in refs. [1,4] and confirmed by the above analysis, prompts the

idea that following their fate can be more useful for (for example) predicting scaling and planning mitigation.

3.1 Scaling with pulse energy

The work of Chen and Wilks [8] explored the energy / temperature of the electrons emitted from a pulse shot of 97mJ on thin Al foil and obtained a quasi-thermal spectrum with a temperature of 120keV. There is also evidence in their plot [8] of a small cohort of higher temperature electrons. Examining possible mechanisms for the acceleration they follow previous work [9,10] in proposing that the electron temperature in high intensity laser shots on foil targets scales as approximately the square root of the intensity. The TITAN measurements of peak EMP electric field strength vs. pulse energy [1] shows fairly erratic results but a general trend consistent with a ½ power law could plausibly be postulated. It would be interesting to see a corresponding plot with the electron temperature replacing the electric field.

3.2 Target size effects

The TITAN results show that increasing the target foil size from 0.4mm to 10mm significantly increases the EMP [1] and Figure 9 shows that the high temperature electrons behave similarly. A possible explanation for this may be that as the capacitance of the target increases the potential well created by the Ag ions decreases and the mean energy of the electrons and rises. It is interesting to note that while the total electron count of the fits to the four different target sizes in Figure 2 are very constant (to within 1%) the fitted T_H is quite erratic and the consistent behaviour of Figure 9 results from using the bunch time spectra. This seems to suggest that electrons of energy around the crook in Figure 2 (~3MeV) are determinant and the exact shape of the high energy part of the spectrum is irrelevant. This is not at all surprising as the electrons are sufficiently relativistic to have essentially all the same velocity. By contrast a rise in the target capacitance would decrease the potential developed across the system and would therefore be expected to reduce the EMP. The fact that the reverse happens tends to reinforce the conclusion that the high energy electrons are a strong determinant of the EMP.

4. Mitigation

The strong implication of the above analysis is that the EMP and the RFI that results from it is an inevitable consequence of the production of copious quantities relativistic electrons in petawatt laser shots. These electrons seem to be an intrinsic feature of all the main applications envisaged for the ELI lasers and therefore have to be accepted as an operational given which will become more troublesome as the laser intensity is ramped up during development. This means that mitigation is the only practical strategy for dealing with the problem. RFI is a form of pollution and like all such problems is most cheaply and efficiently dealt with as near the source as possible – the further any pollution spreads (in general) the greater the cost and difficulty of treating it successfully. In the present case this council of perfection means turning attention to the suppression of the EMP in the target chamber. Attempts have already been made in this direction by the employment of a beam catcher [1] but the results

were not encouraging with a mere factor of 3 reduction in the EMP amplitude. Studying this case can help to point the way to possibly more productive strategies.

In the TITAN studies [1] a spherical "beam dump" was installed consisting of a substantial spherical enclosure of (by estimation from the photograph in ref. [1]) ~50mm radius (made from Al?) with a large slot to allow beam and diagnostic access. A copper strap provided a solid return path to the target holder. The reason that this construction had little practical effect can be appreciated in terms of the above analysis. First, the beam dump itself is a pretty efficient spherical resonator in spite of the copper strap and the aperture. Putting its dimension into the formula found in ref. [5] shows that the lowest modes are E_{1m1} at 2.62GHz and H_{1m1} at 4.28GHz. Turning to Figure 10 we see the relativistic compression shortening the bunch in proportion to the flight path. Thus at 5cm flight to the wall of beam dump, even the slow components are delivered in <500ps while the width of the relativistic spike is almost certainly determined by the acceleration process in the picosecond range. In addition the time delay between the electrons and their induction pulse is reduced pro rata with the flight path. In other words we have set up a system tuned to oscillate at very high frequencies which will beam out microwaves through the slot and also drive the various structures in the target chamber with down-shifting of the RF energy.

The corollary of all the above discussion is that for PW-class lasers the target chamber can no longer be treated as a convenient metal box whose design criteria are related only to the practical requirements of the experiment. It must also be regarded as an RFI generator the suppression of which is one of the primary design criteria. Protection of internal diagnostics is possible with hermetic shielding but the continuation of the shield to include remote receivers is not a trivial matter and if done badly will further spread the RFI. All aspects of the problem become easier if the RF is contained and absorbed within the target chamber. Containment means the design of ports so that windows are RF reflectors. This is not demanding in the GHz region as transparent metal films are efficient. For the lower frequencies keeping the port diameters as small as possible utilises the poor transmission efficiency of apertures smaller than the wavelength. Other expedients such as easily closable port covers on set-up and alignment ports can be considered. Where efficient blocking is not possible (e.g. in the main beam access) RF absorber can be used to line a suitable length of the feed pipes on the approach to the chamber.

RF absorption is a standard requirement in many fields, the classic application being anechoic chambers for testing radar and UHF communications equipment. Two main types are available – ferrite which is used for frequencies below 1GHz and pyramidal absorber (usually made from carbon-loaded foam) above 1GHz. The basic rule for the latter form is that the depth of the structure should be $>\lambda/4$. Since $\lambda\sim30$cm at 1GHz and most of the RF energy is above this frequency, lining the inside of the chamber with this type of absorber is not out of the question as only 75mm depth is required. A further use of RF absorber in the chamber could be the packing of all unused space with temporary moveable blocks which can be arranged as needed for any particular experiment.

Turning our attention to the chamber structure we see that constructing it out of highly conducting metal is not at all desirable from the RFI point of view. With modern materials it may be possible to construct a composite structure – basically of carbon

composite with an outer metal skin for containment. Similarly internal structures should avoid metals as far as possible. Building a high resistance into the target support is also a possible advantage. The amounts of charge that must be moved around the system are tiny: micro-coulombs per shot at shot rates currently ~1 per hour and planned for up to a few per second and capacitances are low (pF) so very poor conductance is quite adequate for restoring neutrality in a timely manner.

5. Conclusions

The implications of our analysis of the EMP problem in PW-class laser shots is that for good operation into the future as the power limits rise the target chamber must change from a "simple" box into a sophisticated RFI suppressor system. The chamber thus becomes an essential element of the Laser Facility and must be managed by it and used by experimentalists under strict criteria. This conclusion is obviously extremely unpalatable to experimenters but seems inescapable. The only method of justifying the validity of this change to them is to perform tests on existing lasers such as VULCAN in order to validate the techniques proposed. RFI reduction is a standard problem and the parameters of the materials available well known. However, adapting them to the high vacuum compatibility standards necessary in laser operations is a matter for R & D.

Acknowledgement

This work benefited from support of the ELI: Extreme Light Infrastructure OP VaVpI project No. CZ.1.05/1.1.00/02.006.

References.

1. Mitigation of Electromagnetic Pulse (EMP) Effects from Short-Pulse lasers and Fusion Neutrons, D C Eder, A Throop, C G Brown Jr., J Kimbrough, M L Stowell, D A White, P Song, N Back, A MacPhee, H Chen, W DeHope, Y Ping, B Maddox, J Lister, G Pratt, T Ma, Y Tsui, M. Perkins, D O'Brien and P Patel, LLNL-TR-411183 (2009).
2. New constraints for plasma diagnostics due to the harsh environment of MJ class lasers, J L Bourgade et. al., Rev. Sci. Instr. **75** (10) 4204, 2004.
3. Operation of target diagnostics in a petawatt laser environment, C Stoecki et. al., Rev. Sci. Instr. 77, 10F506 (2006).
4. M J Mead, D Neely, J Gauoin, R Heathcote and P Patel, Rev. Sci. Instr. 75 (10) 4225 (2004).
5. Wave Guides, H R L Lamont, Methuen, London, 1950, pp 79-81
6. http://mathworld.wolfram.com/BesselFunctionZeros.html
7. J E Bateman, Physics Reports 375 (2003) 411-443
8. Hui Chen and Scott C Wilks, Laser and Particle Beams, (2005) **23** 411-416.
9. Wilks S C et. al. Phys. Rev. Lett. **69** 1383-1386.
10. Wilks SC and Kruer W L, J Quan. Electr. **33** 1954-1968
11. E. Laing, Lectures on Special Relativity, Glasgow University 1962 (unpublished)

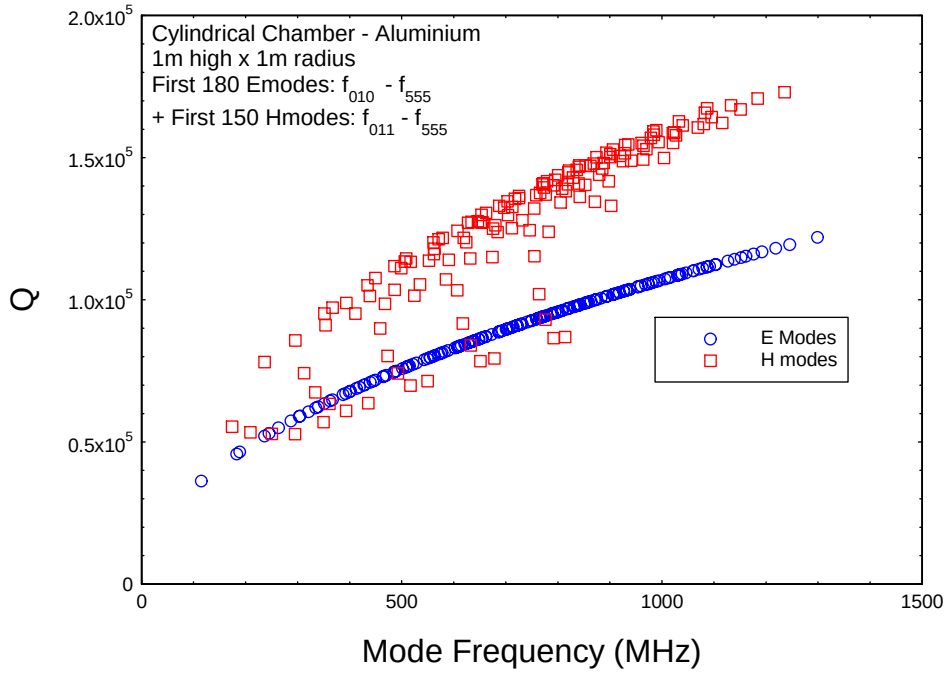

Figure 1. The lowest frequency RF oscillation modes of the model TITAN chamber

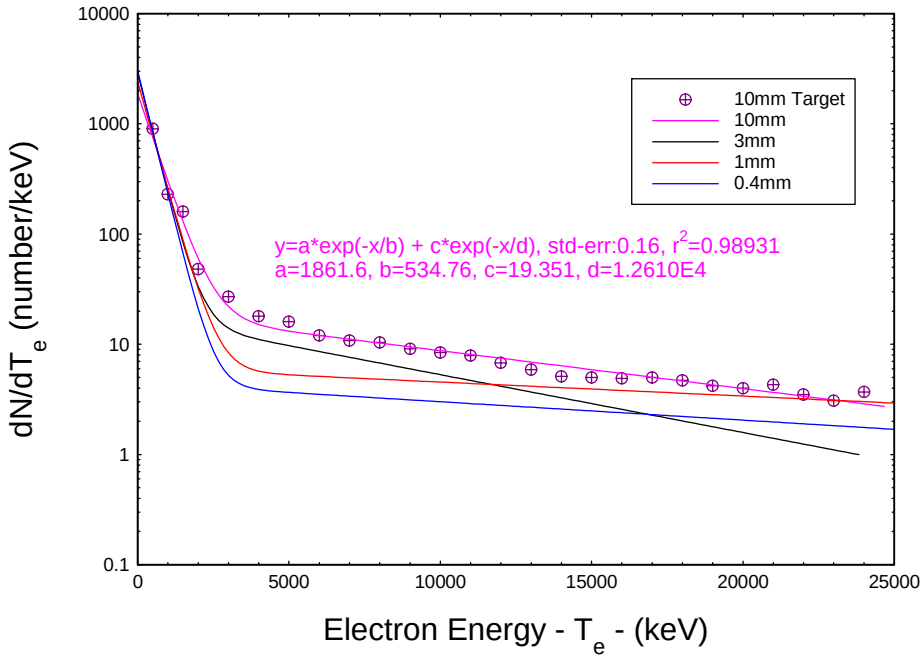

Figure 2. The fitted curves to the electron energy spectra presented in ref. [1]

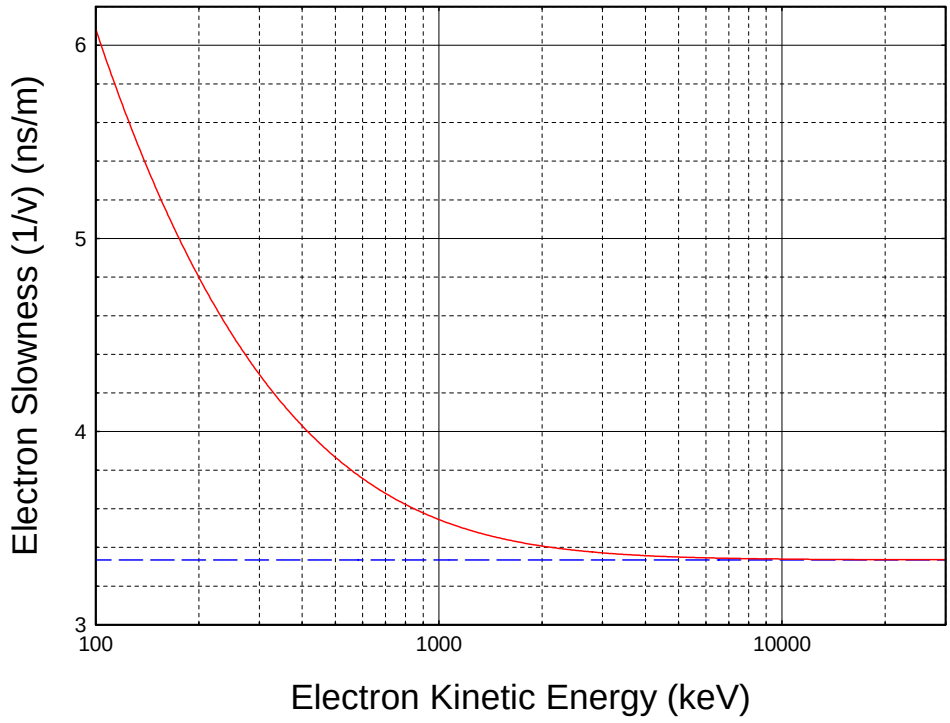

Figure 3. Slowness (1/**v**) of an electron of kinetic energy $\mathbf{T_e}$ in the relativistic region

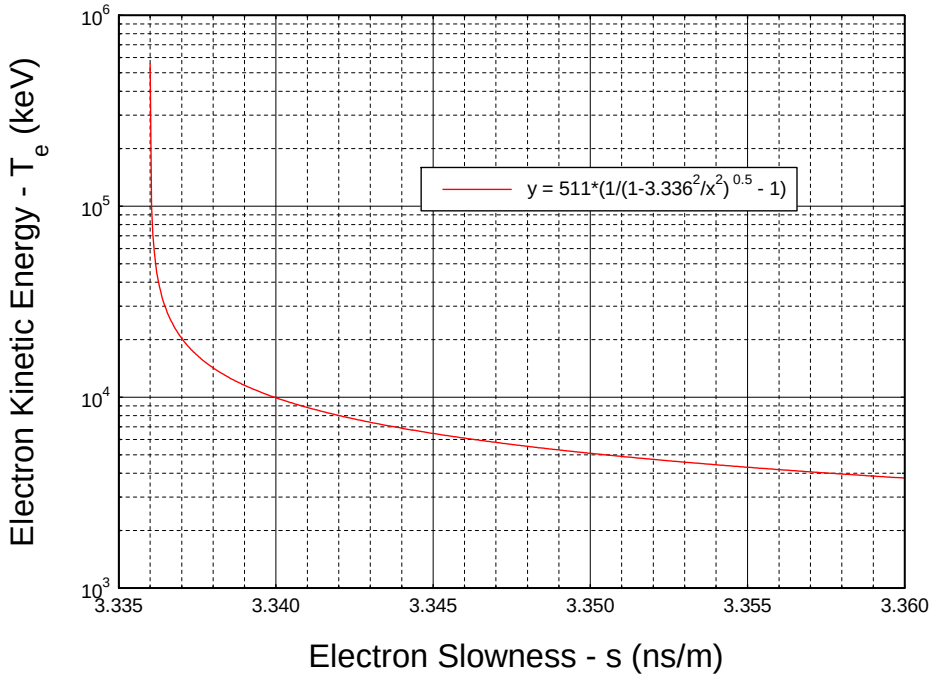

Figure 4. Electron kinetic energy $\mathbf{T_e}$ as a function of its slowness **s**

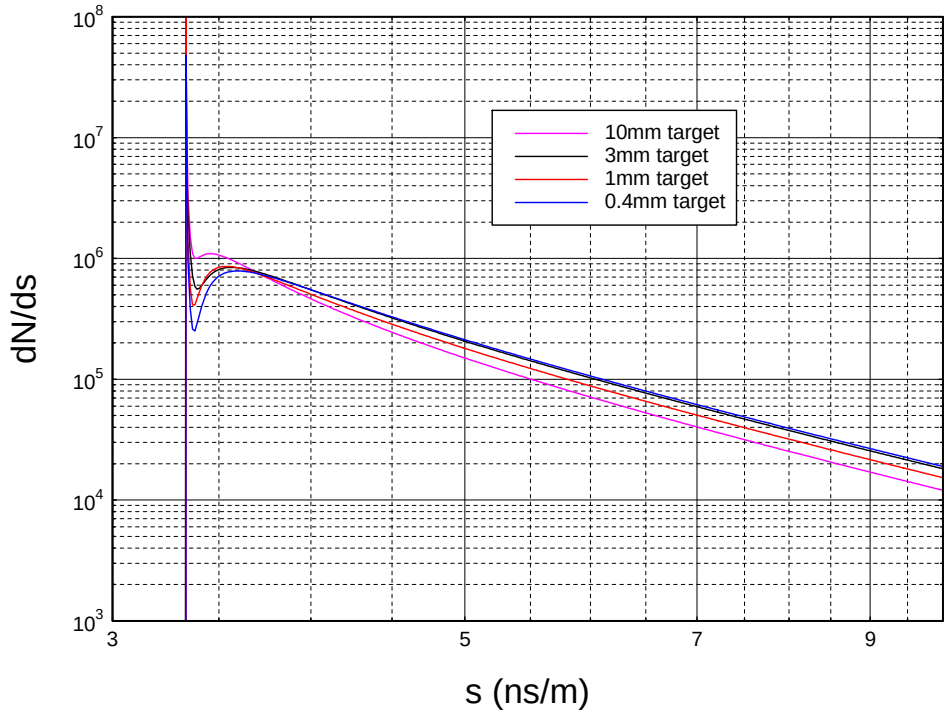

Figure 5. Distribution of electrons in the notional bunch as a function of **s**

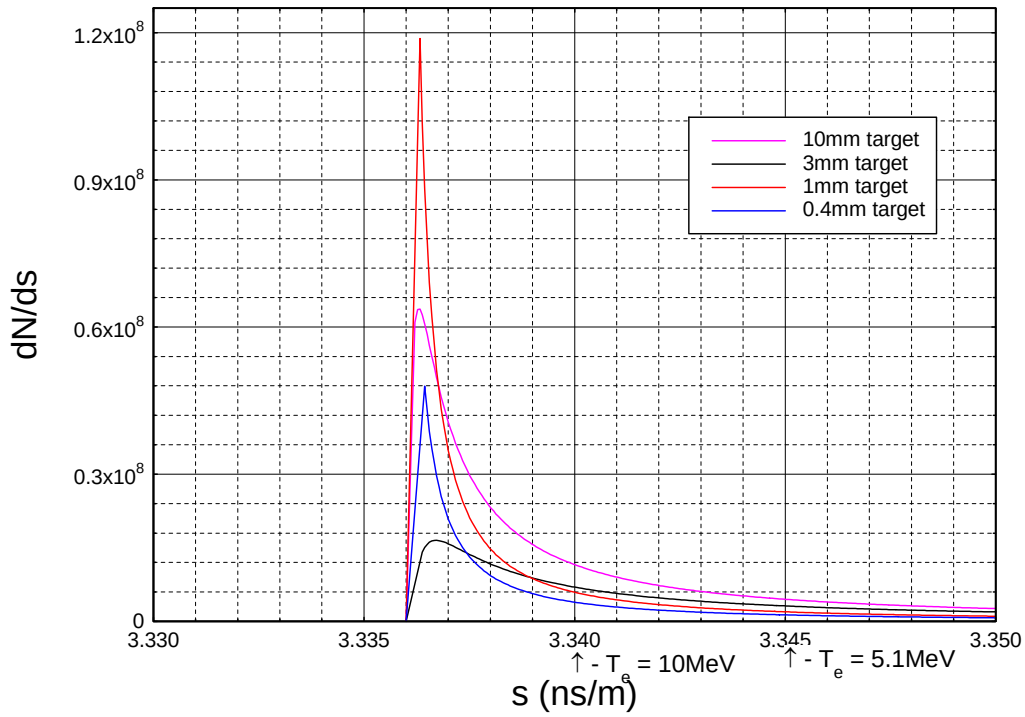

Figure 6. Linear scaled plots of the relativistic spike in the curves of Figure 5

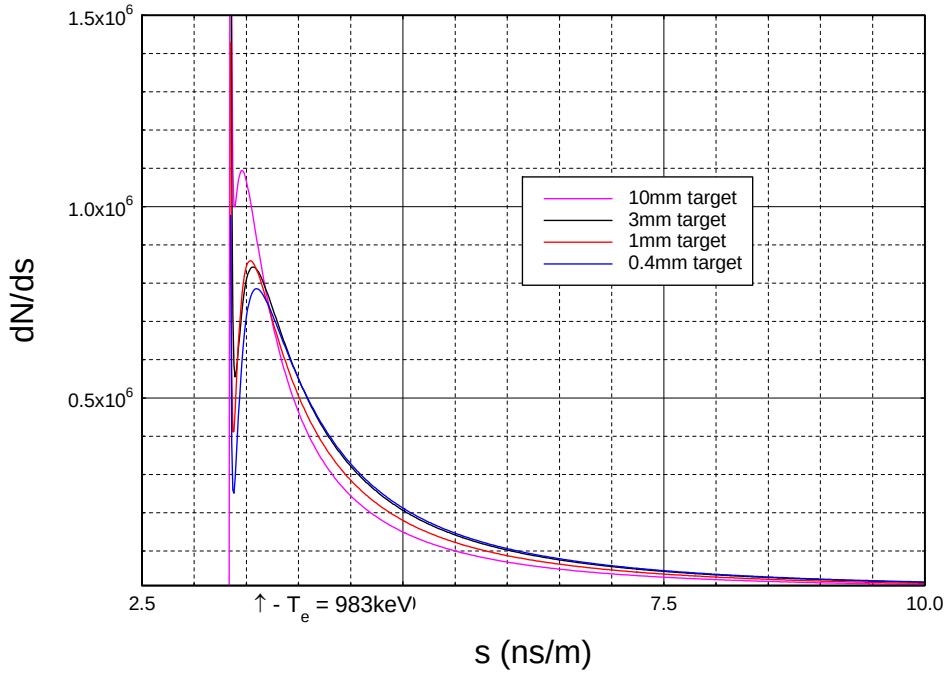

Figure 7. Linear scaled plot of the slower peaks of the distributions of Figure 5

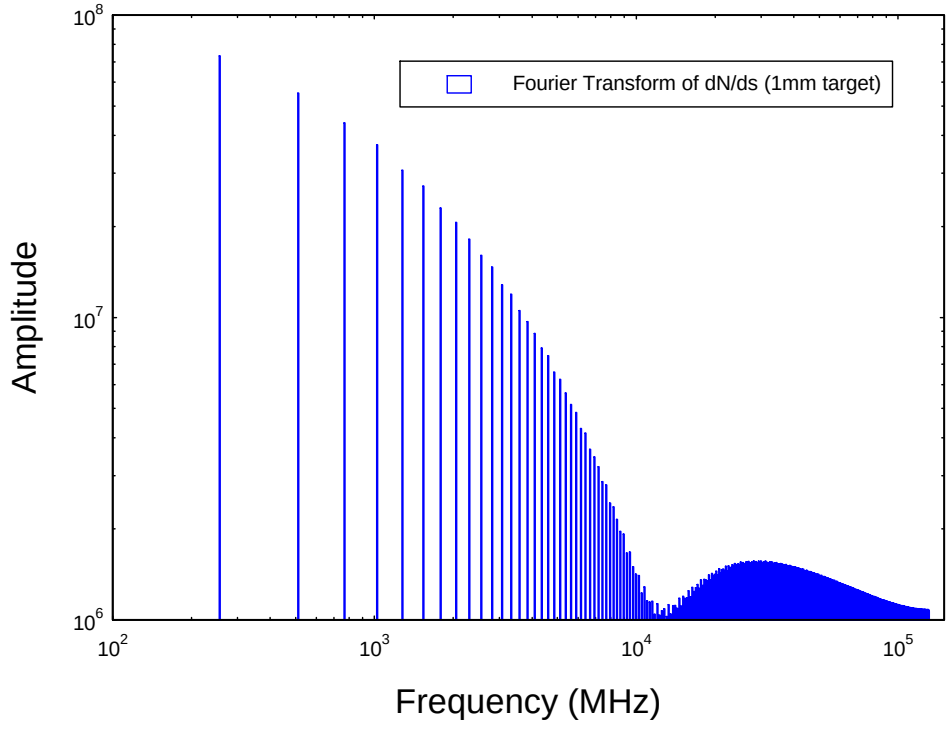

Figure 8. Fourier Transform of the 1mm target plot of Figure 5 (flight of 1m)

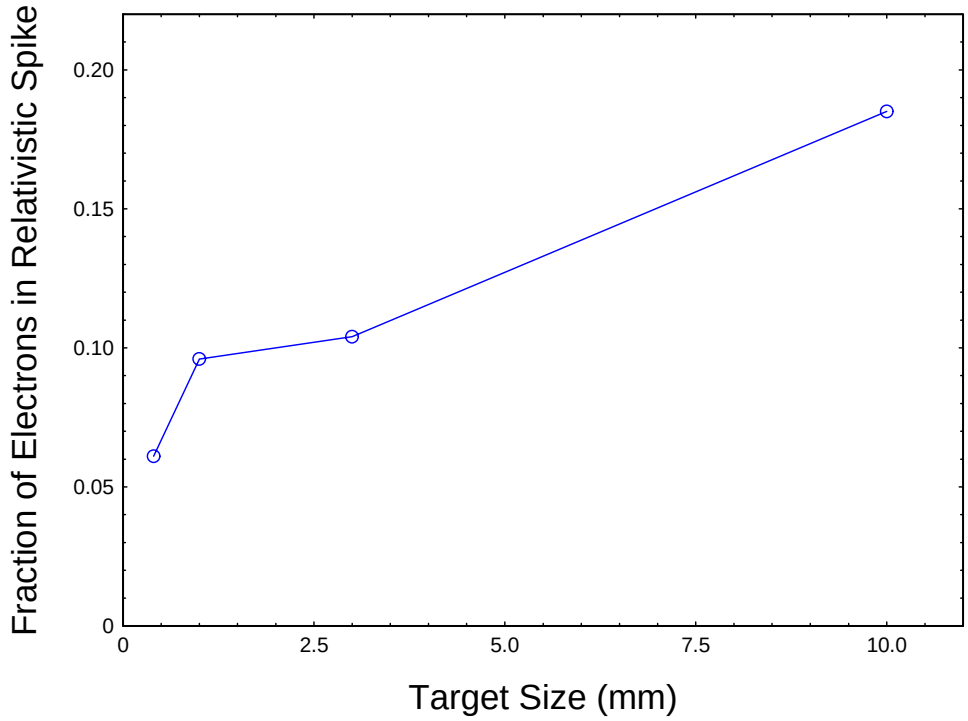

Figure 9. Integrals of the Fig. 6 distributions as a fraction of the total electrons

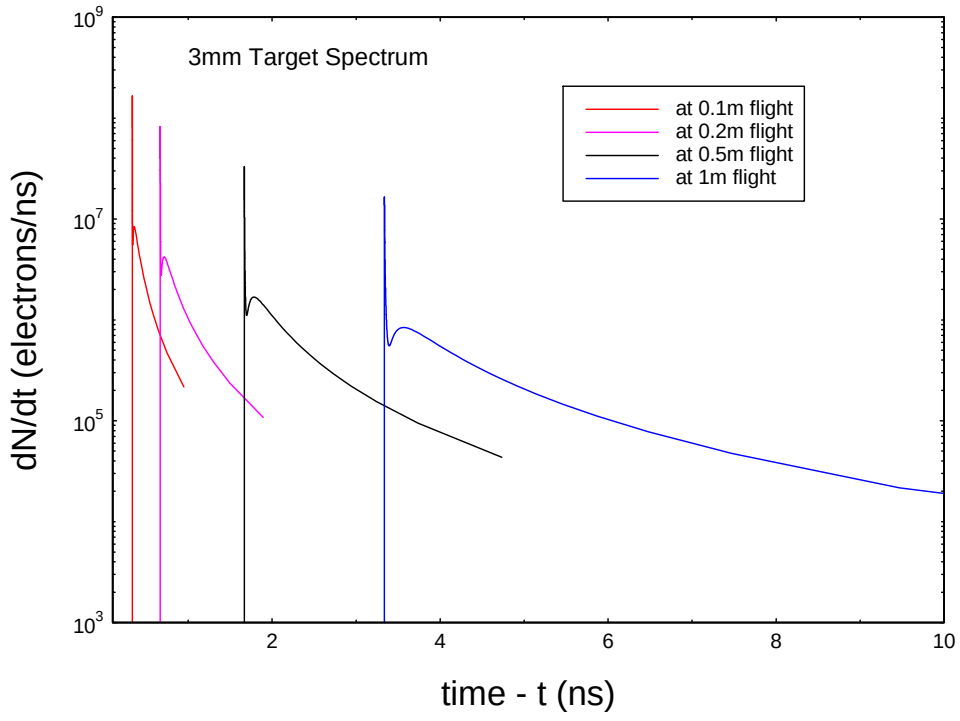

Figure 10. Time distributions of the electrons in the bunch at different flight distances

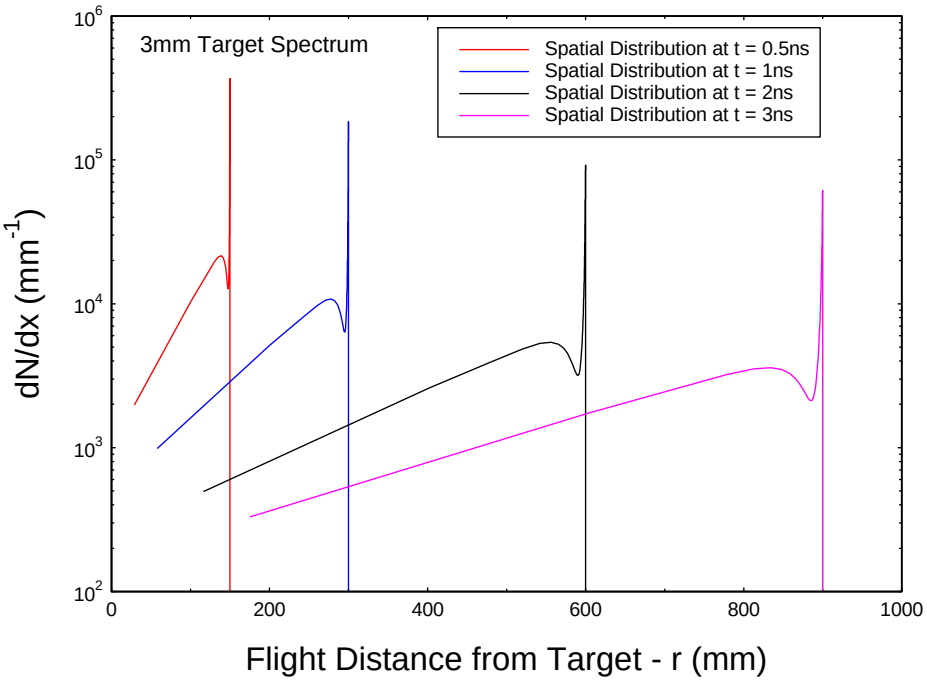

Figure 11. Electron bunch radial profiles at different flight times before wall impact

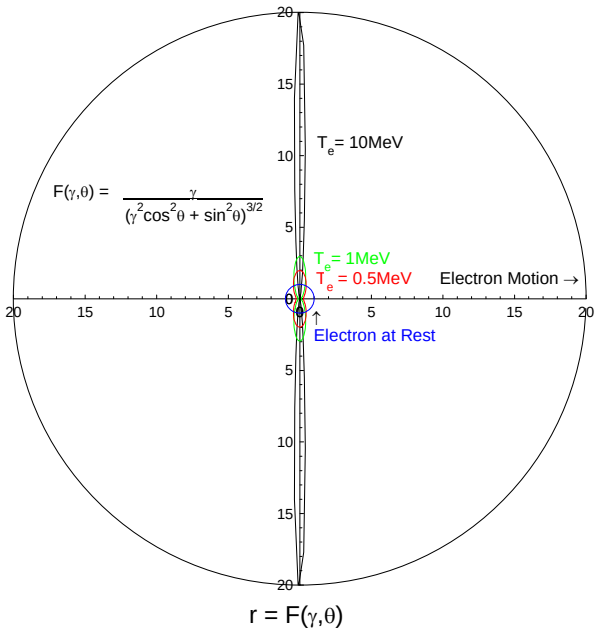

Figure 12. Polar plot of Relativistic Form Factor for the E field of a moving electron.